





Article

An Accurate Probabilistic Model for TVWS Identification

Danilo Corral-De-Witt ^{1,2,*} , Sabbir Ahmed ¹ , Farooq Awin ^{1,3} , José Luis Rojo-Álvarez ⁴  and Kemal Tepe ¹ 

¹ Department of Electrical and Computer Engineering, University of Windsor, Windsor, ON N9B 3P4, Canada; sabbir.ahmed@uwindsor.ca (S.A.); awin@uwindsor.ca (F.A.); ktepe@uwindsor.ca (K.T.)

² Departamento de Eléctrica y Electrónica, Universidad de las Fuerzas Armadas ESPE, Sangolquí 171103, Ecuador

³ Department of Electrical and Electronic Engineering, University of Tripoli, Tripoli 13555, Libya

⁴ Departamento de Teoría de la Señal y Comunicaciones, Sistemas Telemáticos y Computación, Universidad Rey Juan Carlos, 28933 Móstoles, Spain; joseluis.rojo@urjc.es

* Correspondence: corraldd@uwindsor.ca; Tel.: +1-226-246-5278

Received: 16 September 2019; Accepted: 5 October 2019; Published: 10 October 2019



Abstract: Television White Spaces (TVWS)-based cognitive radio systems can improve spectrum efficiency by facilitating opportunistic usage of television broadcasting spectrum by secondary users without interfering with primary users. Previously applied models introduce missed detection errors, giving a limited estimation of the spectrum occupancy, which does not correspond to the reality of its usage, hence resulting in a partial waste of this resource. Considering jointly parameters like false alarm probability and detection probability, this article proposes a probabilistic model that can identify TVWS with improved accuracy. The proposed model considers energy detection criteria, combined with simultaneous sensing of the noise and of the signal from primary users. In order to demonstrate the model effectiveness, a low-cost Mobile Spectrum Sensing Station prototype was designed, implemented, and subsequently mounted on a vehicle. More than eight million spatio-temporally variant data samples were collected by scanning the UHF-TV spectrum of 500–698 MHz in the city of Windsor, ON, Canada. Analysis of the collected data showed that the proposed model achieves an accuracy improvement of about 9.6% compared to existing models, demonstrating that TVWS vary with spatial displacement and increasing significantly in the rural areas. Even in the most crowded spectrum zone, about 28% of the channels are identified as TVWS, and this number increases to a maximum of 60% in less crowded regions in urban areas. We conclude that the proposed model improves the TVWS detection compared with other used models, and also that the elements considered in this research contribute to reduce the complexity of the mathematical calculations while maintaining the accuracy. A low-cost open-source sensing station has been designed and tested, which represents an operative and useful data source in this setting.

Keywords: TVWS; dynamic spectrum access; false alarm probability; detection probability

1. Introduction

Technologies for data-centric wireless communications have experienced an incredible development in the last decade, resulting in huge demands for electromagnetic spectrum. Present spectrum scenarios show a peculiar characteristic, as some bands of the spectrum are extremely crowded, whereas some others are underused. Thus, there is scarcity as well as wastage [1,2]. Smart sharing of the spectrum appears to be a promising solution to this problem. The use of Cognitive Radio (CR) with different sensing techniques allows us to detect unused channels, known as White Spaces (WS), for their opportunistic usage by Secondary Users (SU) without affecting the Primary Users (PU), through a process called Dynamic Spectrum Access (DSA) [3]. In this context, Television White

Spaces (TVWS) are of special interest and this increasingly used term refers to WS that are located in any of the bands assigned to TV-broadcasting service bands [4]. TV spectrum bands often show underutilization by PU and hence the use of TVWS in CR is a promising solution to spectrum scarcity. In this setting, the Institute of Electrical and Electronics Engineers (IEEE) approved the 802.22 standard in 2011 [5]. It is important to note that independently of which spectrum band is being used, CR must avoid interference with PU at any time. But even before that, the task of finding a model that allows accurate identification of TVWS minimizing false alarms errors needs attention.

In this article, we propose an accurate statistical model to identify the presence of TVWS based on the False Alarm Probability (P_{fa}) and on the Detection Probability (P_d). These parameters are obtained by simultaneous sensing the noise intensity ($W(f)$) and the signal of the PU ($X(f)$) in the environmental spectrum. The functional block diagram representing the system that corresponds to our proposed model is shown in Figure 1. As observed, $W(f)$ and $X(f)$ are the two inputs to the collection block where data processing takes place. Next, the processed data is fed to the analysis block, where all the stochastic and mathematical analyses are performed. Then follows the decision block, where the presence or absence of the PU is decided. Finally, results are visually demonstrated in the results block. As finally concluded, this model gives about 9.6% increase in P_d compared to other existing models. The motivation behind undertaking this research endeavour is the fact that CR TVWS has a huge potential in many diverse wireless services and applications, for example, internet access for rural areas, Wireless Regional Area Networks (WRAN), Wireless Sensor Networks (WSN), Emergency Communications (EC), and Telecommunications for Disaster Relief (TDR), among many others. Particularly, the last two applications (i.e., EC and TDR) have drawn significant research interest as they are both related to rescuing lives.

The rest of the manuscript is organized as follows. Section 2 provides a review of the background for this research. Section 3 is a description of the used hardware and data collection patterns. Section 4 describes the proposed model and the mechanism to find TVWS. Experimental results are shown and discussed in Section 5. Conclusions are presented in Section 6.

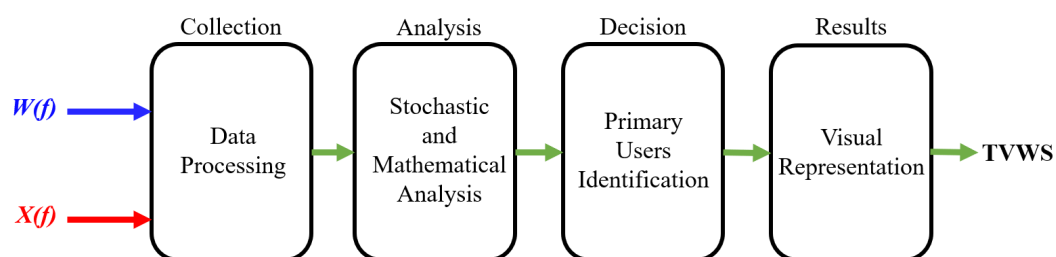


Figure 1. Block diagram of the proposed model.

2. Background

The term CR was coined by Joseph Mitola in his 1999 work [6]. The author described therein how CR could enhance the flexibility of personal wireless services through the so-called Radio Knowledge Representation Language (RKRL). CR is often described as a “disruptive, but unobtrusive technology” [7]. It is disruptive because it allows a SU to access the PU bands, and it is unobtrusive due to the control of different parameters, such as access or transmission power, which dramatically reduces any harmful interference with the PU.

Looking at the current spectrum scenario, we find that the use of unlicensed bands are seen almost everywhere, especially because of the numerous services available to hand-held wireless devices, including Industrial, Scientific, and Medical (ISM) band at 2.4 GHz and the National Information Infrastructure (U-NII) band at 5.2 GHz. This is actually a reflection of how much today’s society is dependent on wireless spectrum [8]. To access and use these open bands, the user does not need to pay any fee or to ask for a license with the local regulator, and more, these bands have similar counterparts around the world, with international regulatory bodies working to align bands and regulations [9].

The common use of unlicensed bands and the development of new devices and technologies led regulatory bodies like the FCC to consider opening further bands for unlicensed use. As stated by the Journal of Communications, “Whereas, spectrum occupancy measurements show that licensed bands, such as the TV bands, are significantly underutilized” [8]. In simple words, what CR is allowing an unlicensed user is to use licensed bands in the very same manner the user would use unlicensed bands, i.e., no fee or no license required. As an alternative to using unlicensed bands, CR is considered the solution to the spectrum wastage due to low usage of the licensed radio spectrum [7]. This technology works on the principle of adapting the operating parameters of the radio according to the conditions of the environment. Thereby it facilitates smart, efficient, and reliable spectrum usage through identifying and exploiting a large amount of unused or underused spectrum bands.

In May 2004, the Federal Communications Commission (FCC) of the United States, proposed the creation of the 802.22 workgroup (WG) for Wireless Regional Area Networks (WRAN). The WG’s goal was to develop the PHY and MAC air interfaces to allow unlicensed users or SUs to operate in the TV broadcast bands without interfering with the PU [10]. During this time, researchers developed spectrum sensing techniques and simulation models, and the idea of smart spectrum gained much interest [5,11]. In 2011, the IEEE 802.22 WRAN standard was approved, which defined a worldwide standard air interface based on CR techniques for the TV broadcasting band [8,12]. Following these guidelines, researchers are considering nowadays different methods to identify idle channel within TV bands or in general within any band. In [13], a detailed list is given with works that use different parameters to identify occupied vs. available channels. These include, for example, statistics with power detection, occupation and duty cycle, Probability Density Function (pdf) or Cumulative Density Function (CDF) with power detection, Markov chains, linear regression, and spectrum prediction, among others. In [14], the authors proposed a spectrum scanning method based on Bayesian inference to estimate the channel occupancy rate, by considering the false alarm and detection probabilities. This approach showed better accuracy compared to other works considering only energy detection to define the presence or absence of a PU.

Based on our analysis of the above mentioned works, we propose that at least three parameters should be considered in each geographical location to evaluate a TV channel, namely, the real instantaneous noise signal, the composite signal consisting of users’ signal and noise, and the energy detected in each reading. These parameters ensure the accuracy of the detected channels and can be used to apply or adapt the IEEE 802.22 standard in current CR systems.

2.1. Cognitive Radio Fundamentals

The functionalities of CR [15] are the following. First, spectrum sensing refers to identify the available spectrum channels and detect the presence of PU operating in a licensed band. Second, spectrum management is the possibility to select the best available channel from all the idle channels detected. Third, spectrum sharing refers to coordinate the smart access to a channel assigned to a PU when it is unused. Fourth, spectrum mobility is the option to vacate the channel when a PU is detected.

According to the definition given by the FCC, A Cognitive Radio is a radio that can change its transmitter parameters based on interaction with the environment in which it operates [16]. From this definition, CR has two characteristics, namely, cognitivity and reconfigurability. **Cognitivity** is the possibility of the device to sense the spectrum. This is not the simple monitoring of the power in a determined frequency band, but rather it requires more elements to identify the temporal and spatial variations in the radio environment, all the time avoiding harmful interference to PU or to another SU. With this, it is possible to identify the unused channels or WS at a specific time or geographical location, giving the possibility to select the best operational parameters [7]. **Reconfigurability** is the capability that permits a dynamic reconfiguration of the operational parameters according to the radio environment. In other words, CR devices can transmit and receive on a variety of frequencies with different access technologies, thanks to their dynamic hardware features [17].

The cycle of the CR is depicted in Figure 2. A portion of the spectrum in a time period t_i is represented, with the signals of the PUs in orange, and the TVWS in white. The first step consists in sensing the spectrum, then this information is analyzed, and based on the obtained result, the device decides which TVWS is the best option to transmit its information. This research is focused on the spectrum sensing and spectrum analysis stages of the CR cycle, specifically in the composite signal that contains the PU information.

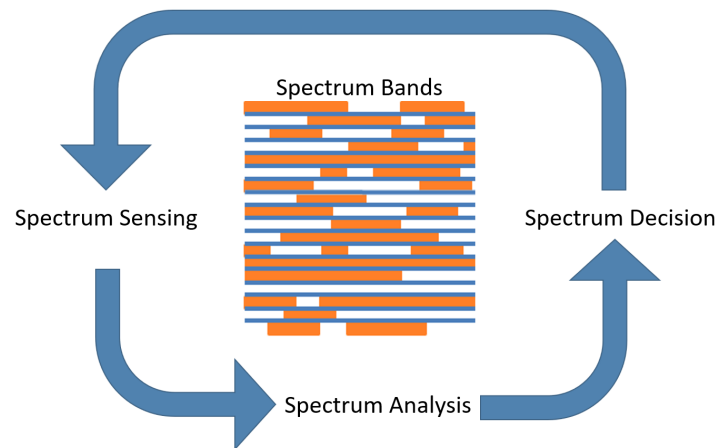


Figure 2. In the Cognitive Radio (CR) cycle, the UHF-TV spectrum band is sensed, then subsequently analyzed, and a decision is taken based on the presence or absence of Primary Users (PUs).

2.2. TVWS Basics

As mentioned before, the unused and underutilized frequency spectrum spaces are referred to as WS. Efficient utilization of these WS has the potential to reduce the spectrum scarcity faced nowadays with the fast growth of wireless technologies. According to [18], the characteristics of the WS are: (i) A white space is an unused radio frequency; (ii) Its existence depends on time, frequency, and geographical location; (iii) Its utilization should not cause any harm to the PU. These concepts are known as TVWS when applied to the TV broadcasting frequencies.

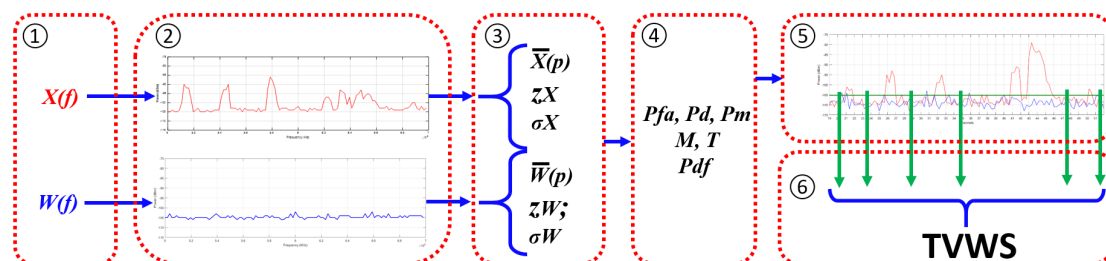
In this research, we are interested in the frequency bands assigned to the TV service. Table 1 illustrates the frequency ranges, channel numbers, bandwidth for each band, and the respective ITU regions [19] where the bands are allocated. Our work focuses on bands IV and V, i.e., 500 MHz to 698 MHz [20,21]. It should be noted that channel 37 (608 MHz to 614 MHz) is used for radio astronomy and it is excluded from TV broadcast services. The three main reasons to choose said spectrum bands are explained next. First, the propagation characteristics of frequencies under 1 GHz are favorable for robust transmission, and there are standards as IEEE 802.22 considering the TV band to access as a SU. Being recommended by an organization like IEEE, regulatory bodies across the globe have started applying them in their territories [5]. Second, the selected range of frequencies offers 198 MHz (32 channels) of continuous spectrum, except for channel 37. This spectral continuity gives more possibilities to find and use idle channels without major modifications in the transmission parameters of the antennas. Third, multiple studies have demonstrated that there is a significant number of underused TV spectrum bands even in urban areas, and their availability increases rapidly in rural areas [18].

Table 1. Bands assigned to the TV broadcasting service, and their corresponding frequencies, channel numbers, partial Bandwidth (BW), and ITU regions.

Name	Frequencies	Channels	Partial BW	ITU Regions
Band I	54–72	2 to 4	18 MHz	R1, R2, R3
Band I (Cont.)	76–88	5 to 6	12 MHz	R2
Band III	174–216	7 to 13	42 MHz	R1, R2, R3
Band IV	500–644	19 to 42	144 MHz	R1, R2, R3
Band V	644–698	43 to 51	54 MHz	R1, R2, R3

3. Prototype Description

Before describing the prototype and its hardware configuration, it is necessary to review the proposed model. Six blocks are visualized in Figure 3, starting with block ① that refers to sensing the information of the composite signal $X(f)$ and the noise signal $W(f)$ in a separate manner. Block ② refers to how the samples obtained are processed by each device, i.e., the RF Explorer (RFE) and the Spectrum Analyzer (SA). In block ③, the statistical parameters of each sensed signal are calculated and saved. Block ④ shows the calculated P_{fa} , P_d , Missed-detection Probability (P_m), the optimum values for Margin (M), and Threshold (T), and other information needed to analyze the UHF-TV spectrum. Block ⑤ features the Energy Detection (ED) procedure to identify unused channels and PU's presence. Finally, block ⑥ explains how the output information is represented, detailing the amount of TVWS. Based on this model, the prototype must consider the elements listed in Table 2.

**Figure 3.** Chart flow of the proposed model.**Table 2.** Hardware measurement setup of mobile spectrum sensing station.

Ord	Device	Observation
1	External Antenna	Omni, 5 MHz to 1000 MHz range
2	GPS Antenna	USB connector
3	Attached Impedance	50 Ω
4	RF Explorer	Sub 1 G, 240 MHz to 960 MHz range
5	Spectrum Analyzer	High accuracy, 50 KHz–3 GHz
6	Portable Computer	Hardware and software needed
7	External Hard Disk	To save readings and information

We designed a Mobile Spectrum Sensing Station (M-SSS) to measure TVWS over the UHF-TV spectrum in the city of Windsor and surroundings. Figure 4a shows that the M-SSS is composed of two Data Acquisition Instruments (DAI), in this case, two RFE installed in parallel, one device connected to a Winegard antenna to collect information of the composite signal $X(f)$ and the other device with a 50 Ω impedance attached and used to sense the noise of the system $W(f)$. These devices are employed to detect the energy of TV signals over the UHF band. This mobile configuration also has attached a GPS antenna to collect the geographical location for each reading.

The M-SSS was designed to be mounted on a vehicle. For this, a supporting structure was assembled using a plastic pipe that fits in a Dodge Grand Caravan vehicle, as shown in Figure 4b–d.

The antenna and the designed structure, support a speed up to 120 Km/h, verified, and theoretically, a speed up to 144 Km/h, according to data provided by the manufacturer.

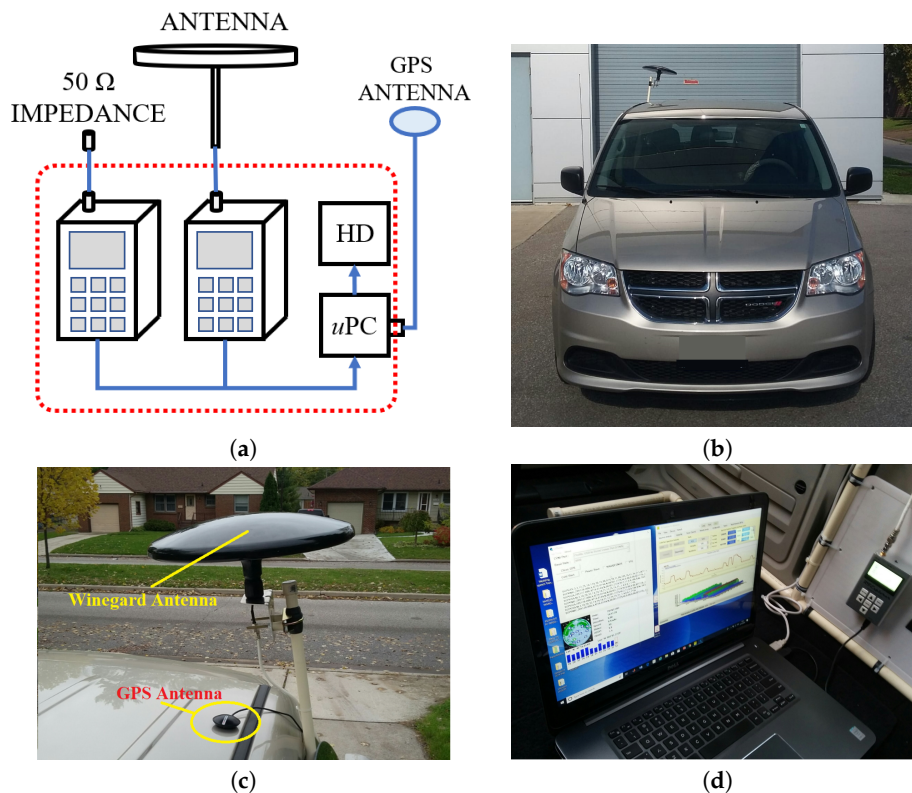


Figure 4. Mobile Spectrum Sensing Station (M-SSS) designed to be mounted on a vehicle and sense the TV spectrum in wide geographical areas: (a) Diagram of the M-SSS; (b) Mounted station; (c) Winegard and GPS antennas; (d) M-SSS in operation.

We used two antennas in our system, a Winegard antenna, model MS-3005 VHF/UHF, 14.9', and a Global Sat BU-353-S4 USB low consumption GPS antenna. The Winegard MS-3005 is an omnidirectional antenna for receiving VHF and UHF-TV channels. Its frequency range is from 5 MHz to 1000 MHz. It can be installed in indoor or outdoor environments, and we used it to collect information with the designed M-SSS. Two Winegard antennas were used in this research, one installed on the laboratory roof and another in the M-SSS, both aimed to collect information of the UHF-TV spectrum. The GPS information was collected with a BU-353-S4, which is a low power consumption device enclosed in a compact magnetic body, and it can be placed on the vehicle to receive the information of the Global-Sat constellation GPS satellites and save it in our Database (DB).

The RFE Sub1G device is a low cost, open source, and portable spectrum analyzer designed for the specific needs of digital radio frequency communication. It supports the detection of expected transmission power, automatic resolution of Resolution Bandwidth (RBW), sweep time, and spectrum data calculations. Moreover, it also has the features of real-time or adjusted signals, 3D spectrogram waterfall, CSV export, and high-quality graphics. A large number of feature sets can be applied and controlled through cooperated work between the RFE and Windows on the Personal Computer (PC) [22]. Two of these RFE devices were used in the M-SSS, one to collect noise samples and another to sense the composite signals, and both readings were sensed in each location. Its technical characteristics are the following:

- Frequency Range 240 MHz to 960 MHz.
- Span 0.112 MHz to 300 MHz.
- Frequency Resolution 1 KHz.

- Average Noise Level –115 dBm.
- Amplitude Resolution 0.5 dBm.
- Automatic RBW 2.6 KHz to 600 KHz.

The Tektronix MD04054-3 SA was used in this project, with the purpose of verifying the accuracy and quality of the readings taken with the RFE, and visualizing the obtained data. It is an oscilloscope with a built-in spectrum analyzer [23], allowing to capture time-correlated analog, digital, and RF signals. Its technical characteristics are:

- Frequency Range 50 KHz to 3 GHz.
- Bandwidth 500 MHz.
- Span 1 KHz to 3 GHz.
- Frequency Resolution 20 Hz to 10 MHz.
- Average Noise Level –115 dBm.
- Amplitude Resolution 0.5 dBm.
- Automatic RBW 2.6 KHz to 600 KHz.

By using the M-SSS, we measured the power level of the UHF-TV spectrum in the city of Windsor, following four trajectories. The samples were taken continuously along the sensed area. The RFE device scans 198 MHz bandwidth of the 500 MHz to 698 MHz UHF-TV spectrum with a separation of 1.76 MHz at a given time instance. This means that there are $198 \text{ MHz} / 1.76 \text{ MHz} = 112$ samples reading per RFE at a given time instance. Along with two RFE devices, we used one GPS device. Hence, a single reading constitutes of 112 Signal power in dBm, 112 Noise power in dBm, and 1 location-timestamp data samples. The RFE devices took readings every 0.340s which implies that for a duration of 1 minute, we had $(112 + 112 + 1) \times (60/0.34) = 39,705$ data samples. The relevant data collection setup parameters are listed in Table 3, which shows that there are 36,176 readings representing 4,051,712 samples per RFE. Since there are 112 samples per reading, in total 8,103,424 samples were collected. The time interval between each reading was 0.340 seconds. The signal and noise data samples, along with the GPS information of Latitude and Longitude, were saved in the DB of the M-SSS.

Table 3. Number of readings and samples collected with each RF Explorer (RFE).

Trajectory	Distance in Km	Readings	Noise Samples	Signal Samples
T1	16.05	5417	612,752	612,752
T2	32.45	10,419	1,166,928	1,166,928
T3	31.48	12,924	1,447,488	1,447,488
T4	23.22	7362	824,544	824,544
Total	103.20	36,176	4,051,712	4,051,712

4. Proposed Probabilistic Model

This section provides a brief explanation of the probabilistic model developed to address the research objectives. We start by analyzing how to calculate the reference noise level. Then a brief review of M and T proposed by other authors, together with the parameters considered to calculate T , are detailed. The normality of the used distributions and the applicable tests are also included. Then, attention is paid to obtaining the pdf from the collected data, the used performance metrics, how to calculate P_{fa} and P_d , their maximum and minimum values, and how these values are related among them.

4.1. Sensing the TV Signal and the Noise

The existence of the PU can be modeled by using the following hypotheses in the frequency domain:

$$H_0 : X(f) = W(f) \quad (1)$$

$$H_1 : X(f) = S(f) + W(f) \quad (2)$$

where $W(f)$ denotes Additive White Gaussian Noise (AWGN), $S(f)$ denotes the received signal of the PU, $X(f)$ denotes the sensed composite of signal and noise, and H_0 represents the null hypothesis for the of PU absence in the channel, whereas H_1 represents alternative hypothesis of the PU presence in the channel.

By using the designed M-SSS, the information from the UHF-TV spectrum was collected at each instance of time t_i and plotted, as shown by the example in Figure 5. In both cases, for RFE and for SA, the signal presents a similar shape in general terms, with specific frequencies in which the power in dBm rises to its maximum values and other frequencies in which minimum values are reached. These panels show the power variations and differences between them in the time domain, which are due to the internal characteristics of each device.

The information of $X(f)$ alone is not enough to identify TVWS, so that is imperative to find more parameters allowing to identify the presence of PU. A crucial point to be considered is how the noise is measured and its mean $\bar{W}(f)$ is calculated. In the reviewed literature, in some cases, the noise is sensed at the beginning of the measurement campaign and that value is used to be compared with all the readings, in other cases a theoretical value is considered, and a third approach is to consider a fixed threshold T . In practice, it is very difficult to obtain accurate information about the noise power [24] due to its variability or unexpected noise sources along the measured pattern when the samples are taken.

According to the IEEE 802.22 standard [5,10], the channel in operation must be sensed several times, namely, during the transmission, inter-framing time intervals, and in-framing. It is important to obtain trustful and accurate channel noise and signal samples. In order to obtain accurate information regarding the noise, simultaneous sensing of the noise and the signal is here proposed. As it can be seen in Figure 4a, signal $X(f)$ is received through the antenna and sensed with one DAI, and at the same time, another DAI with similar characteristics and a 50 Ω matched impedance is used to sense the noise of the system. As a result, both the signals (i.e., $X(f)$ and $W(f)$) are used in our proposed channel sensing mechanism.

With the mentioned hardware configuration, the UHF-TV spectrum was sensed, and representative examples are shown in Figure 5a,c for the overlapped curves of $W(f)$ in blue and $X(f)$ in red, taken with the RFE and SA, respectively. The next logical step is to calculate the statistical mean of the noise $\bar{W}(f)$ in black, taken with the same instruments at time instant t_i . Note that this is the reference level for calculating T .

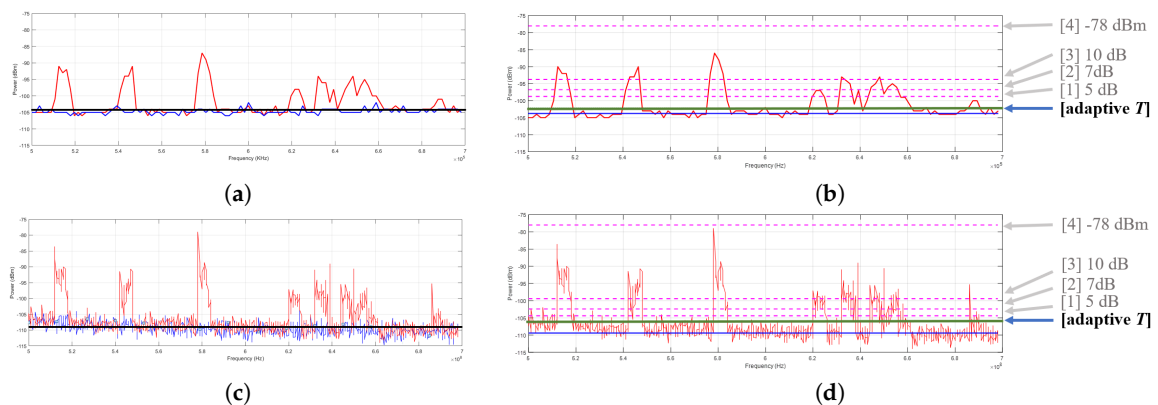


Figure 5. TV signals sensed with RFE (top) and SA (bottom) are compared. The $X(f)$ in red, $W(f)$ in blue, and $\bar{W}(f)$ in black are observed in panels (a,c), $\bar{W}(f)$ is the calculated noise level. In panels (b,d) are plotted $X(f)$, $\bar{W}(f)$, and the different values for M or T .

4.2. Threshold Considerations

As found in the literature of TVWS sensing, the sensed signal $X(f)$ is compared with Threshold T , which is obtained from

$$T = \overline{W}(f) + M \quad (3)$$

where $\overline{W}(f)$ is the average noise floor level in dBm, and M is a margin in dB. Determining a threshold plays a critical role in classifying PU activities as a busy or as an idle channel, i.e., TVWS [13]. Moreover, it is used to determine the duty cycle of the channel which defined as a ratio of the number of sensing samples above the threshold to the total employed sensing samples. Generally, threshold is defined as an average noise floor level plus some margin. Different existing measurement campaigns conducted by other authors, have employed various margin values such as 5 dB in [25], 7 dB in [26], and ITU uses a 10 dB, while the measurement in campaign [27], considered a fixed threshold of -78 dBm. The main reason of considering the margin is samples of noise measurement are not Gaussian distributed, therefore, adding margin excludes a wrong decision of PU existence by not considering noise as a PU signal [25]. In other words, noise samples cannot reach the threshold when adding margin to the average noise floor level, therefore, false alarm will be reduced as only a PU signal can exceed it. However, such thresholds prevent detecting weak PU signals which might result in missed detection, therefore, a margin value should be selected carefully [28,29].

In Figure 5 we can observe $X(f)$, sampled with RFE in panel (b) and with SA in panel (d). Both representations show the previously discussed values M and T . It is obvious from these figures that the higher the chosen value of M , the higher the occurrence of signal missed-detection. In the specific case of $T = -78$ dBm, all the 32 channels appears to be idle, which is not necessarily true because at least 8 signal peaks can be observed. The purpose of sensing and plotting two signals, i.e., $W(f)$ and $X(f)$, is to identify the characteristics of each signal and compare with each other, in order to obtain enough parameters to develop the proposed probabilistic model.

The above discussion reveals that in order to sense the UHF-TV spectrum for accurate identification of idle channels, it is imperative to define an adaptive T . The value of T should satisfy the following conditions: First, it should be close enough to $\overline{W}(f)$ to avoid missed detections; Second, it should be far enough from $\overline{W}(f)$ to avoid false alarms (fa); And finally, it should be adaptive to the possible changes experienced by $W(f)$ and $X(f)$, especially when the M-SSS moves from one to the next location.

4.3. Working with Normal Distributions

In this research, both signals, i.e., the noise $W(f)$ and the composite signal $X(f)$, are collected simultaneously by two RFE devices connected in parallel. To verify that the sensed noise $W(f)$ is a normally distributed signal, two complementary kinds of statistical methods were applied, namely, graphical and mathematical [30,31]. The first one plots the samples of the noise signal, and its distribution is compared with a predefined pattern. Following this method, Figure 6a shows the histogram of the noise samples taken in a particular location and Figure 6b shows the probability distribution plot of the same samples. It is visually evident that the plotted samples correspond to a normal distribution.

The second method is a statistical test; in this case, the Kolmogorov–Smirnov Test (KST) [31], which takes the signal samples and verifies if they follow specific parameters to be considered as normally distributed. This test with a 5% significance level was applied to the collected noise samples, and the corresponding results of the CDF are shown in Figure 6c. These numbers suggest that the tested samples are normally distributed.

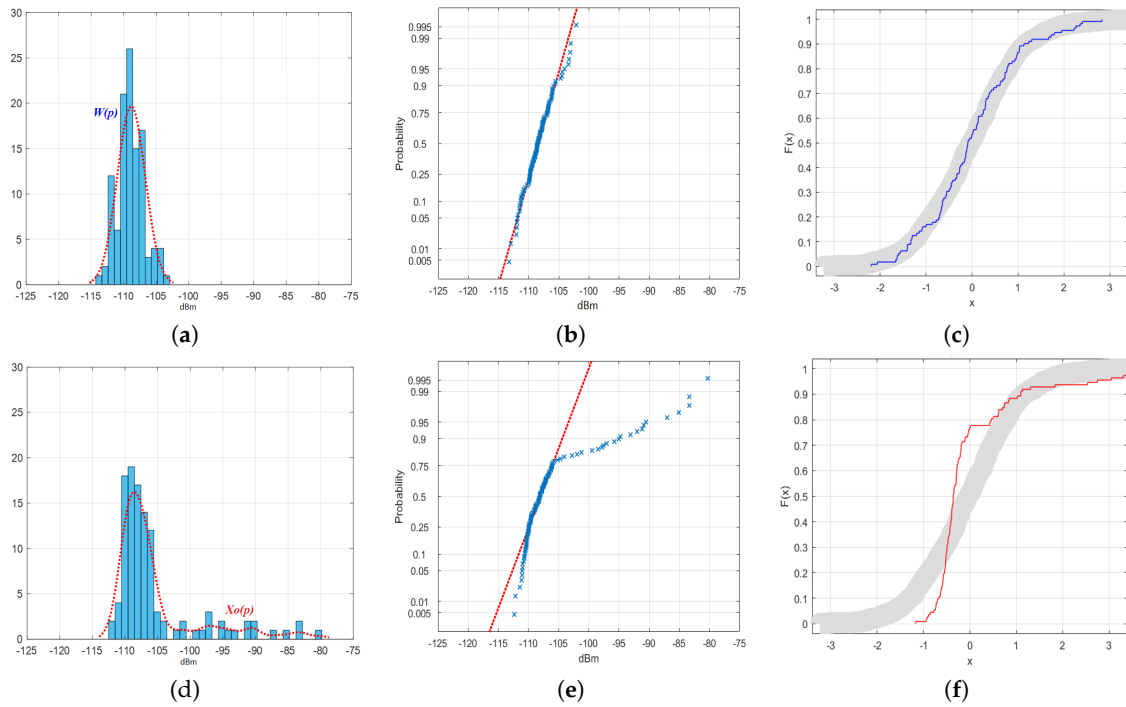


Figure 6. Noise signal sensed $W(p)$. (a) Histogram of the collected data. (b) Normal probability plot of the same data read. (c) Cumulative Density Function (CDF) of the Kolmogorov–Smirnov Test (KST) applied. Curve of the multi modal composite signal sensed $Xo(p)$, (d) Histogram of the collected data, (e) Normal probability plot of the distribution for the same reading, and (f), CDF of the KST applied.

On the other hand, as is shown in Figure 6d,e, the multi modal composite signal $Xo(p)$ presents a distribution in which it is possible to identify the component of noise represented by a higher peak and the signal of PU represented by the multi modes on the right tail. When the KST [31] with a significance level of 5% is applied to the composite signal samples, the results suggest that it does not correspond to a normally distributed signal, as observed in Figure 6f.

In our model, the composite signal with multi modal curve $Xo(p)$ observed in Figure 7a can be represented as the normal distribution curve. Also, $X(p)$ is shown in Figure 7b. By considering the statistical parameters of $Xo(p)$, i.e., the mean and standard deviation, we generate the above mentioned normal curve that fits the sensed multi modal composite signal. In Figure 7c we observe the variations among the multi modal $Xo(p)$ and the assumed $X(p)$ curves. This assumption is necessary to reduce the complexity of the mathematical calculations.

Figure 7 shows the pdf of different signals. The pdf of the noise $W(p)$, the multi modal curve of the composite signal $Xo(p)$, and the normal curve of the composite signal $X(p)$ are plotted in blue, magenta, and red, respectively, for three different locations. Panel (a) shows the curves of the noise $W(p)$, Panel (b) represents the intersection points of $W(p) \cap Xo(p)$ named as A and its projection to the X-axis or A' , and Panel (c) shows the overlapping intersection points of $W(p) \cap X(p)$ named as B and its projection to the X-axis or B' . In these plots, it is easy to observe that

$$A' - B' \ll P(\text{dBm}) \quad (4)$$

which means that A' and B' are very close together, and its difference is minimal compared with the power of the measured signals so that it can be neglected. This fact supports that the multi modal composite signal $Xo(p)$ can be assumed as a normally distributed signal $X(p)$ to reduce the mathematical calculation complexity without affecting the accuracy of the obtained results.

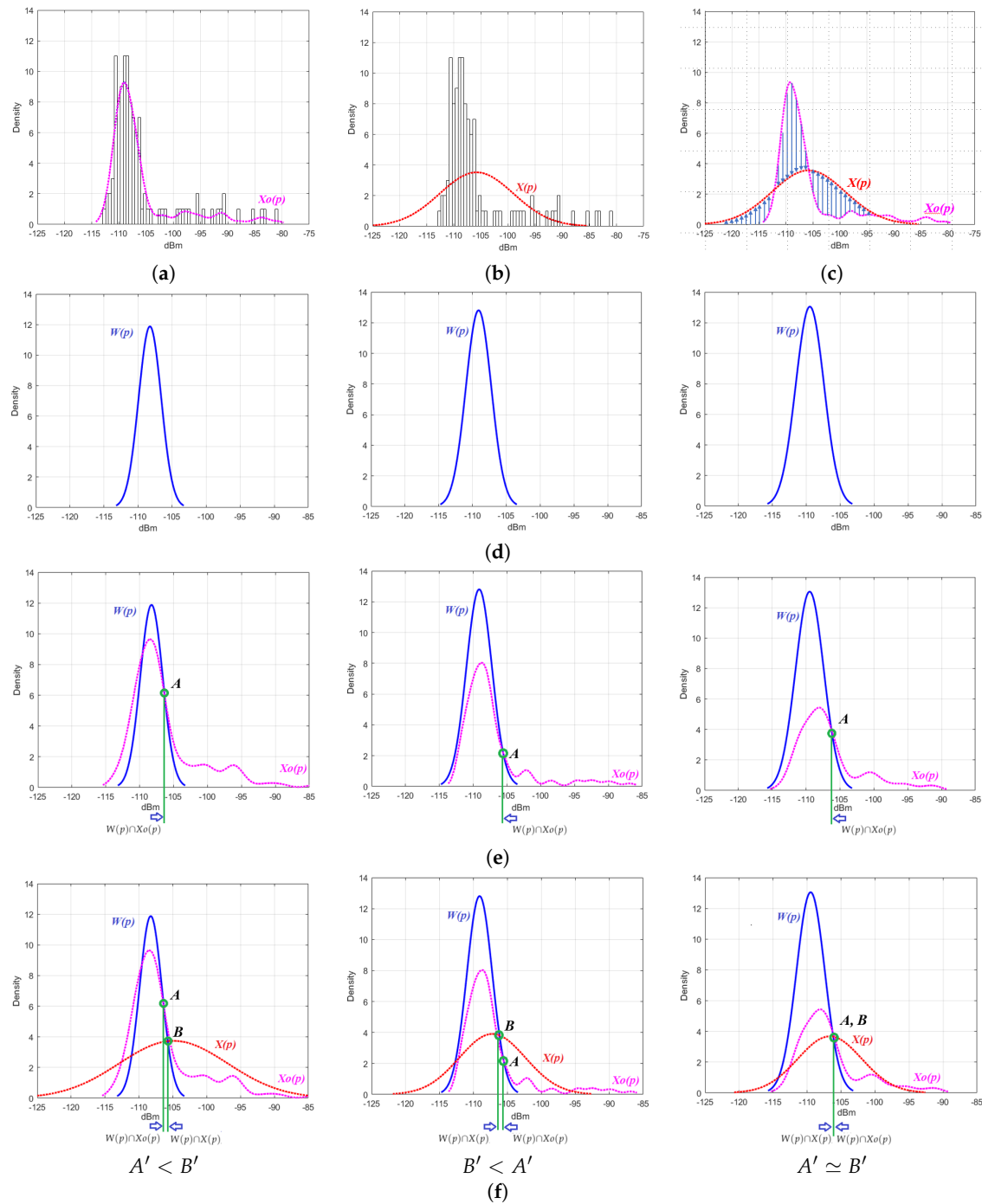


Figure 7. The curve $Xo(p)$ of the multi modal distribution of (a) can be assumed to follow the normal distribution curve $X(p)$ of (b), and this assumption summarized in (c) allows us to reduce the calculation complexity of the proposed model. Readings taken in three different points. The Probability Density Function (pdf) for the noise $W(p)$ is plotted in blue, multi modal composite signal $Xo(p)$ in magenta, and composite signal $X(p)$ in red. In (d), the pdf of the noise for each location are shown. In (e), the intersection point “A” of $W(p) \cap Xo(p)$ and its projection to the power axis “A’” are represented. In (f), the intersection point “B” of $W(p) \cap X(p)$, and its projection to the power axis “B’” are represented.

This assumption is supported by the fact that the calculation of P_{fa} was done on the noise signal, i.e., $W(p)$, which corresponds to a normal distribution. In addition, the following two points should also be noted. First, for calculating P_{fa} , the left intersection point “C” of the pdf of $W(p)$ and $X(p)$

will not be considered here, because it is located below the mean value of the noise signal $\bar{W}(p)$. And second, for calculating of P_d , the right intersection point “B” of the pdf of $W(p)$ and $X(p)$, and the right tail of the signal will be considered. Once these assumptions are adopted, then the pdf that represents the noise $W(p)$ and the composite signal plus noise $X(p)$ are those ones illustrated in Figure 8.

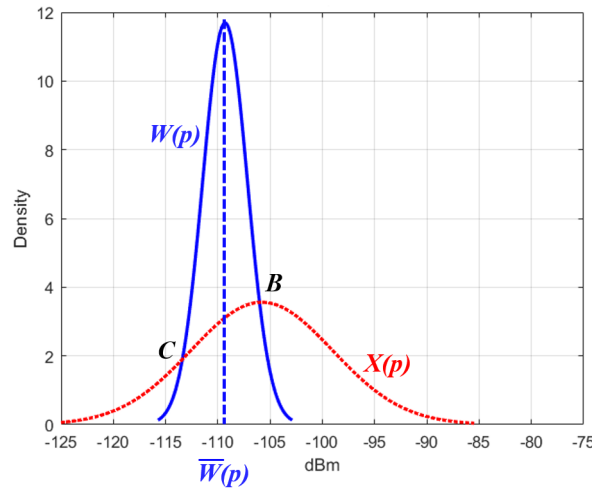


Figure 8. Normal distribution pdf for $W(p)$ in blue and $X(p)$ in red, which are assumed to calculate the P_{fa} and the P_d according to the proposed model.

The frequently used statistical parameters regarding the sensed signals are P_{fa} , P_d , and the missed detection probability (P_m). With the collected information of $W(p)$ and $X(p)$, and considering that both signals correspond to normal distributions, other statistical parameters can be calculated, such as mean values of the signals ($\bar{W}(p)$, $\bar{X}(p)$), or their standard deviation (σ_W and σ_X). An interesting manner to relate the obtained parameters is by using the pdf of the signals, which provides a visual explanation of the proposed method, and it is explained next.

To plot the pdf of a signal that follows a normal distribution, it is necessary to apply

$$f(x) = \frac{1}{\sigma\sqrt{2\pi}} \exp \left\{ \frac{-1}{2} \left(\frac{x - \bar{x}(p)}{\sigma} \right)^2 \right\}; -\infty < x < \infty \quad (5)$$

where σ is the standard deviation and $\bar{x}(p)$ is the mean of the distribution. By taking the samples of $X(p)$ and $W(p)$, the equations that define both pdf curves, are $f(x_W)$ and $f(x_X)$ with $\bar{W}(p)$ and $\bar{X}(p)$ as the means, σ_W and σ_X as the standard deviations respectively, and then the equations are:

$$f(x_W) = \frac{1}{\sigma_W\sqrt{2\pi}} \exp \left\{ \frac{-1}{2} \left(\frac{x - \bar{W}(p)}{\sigma_W} \right)^2 \right\} \quad (6)$$

$$f(x_X) = \frac{1}{\sigma_X\sqrt{2\pi}} \exp \left\{ \frac{-1}{2} \left(\frac{x - \bar{X}(p)}{\sigma_X} \right)^2 \right\} \quad (7)$$

Now, considering Equation (2) that shows the composite signal consisting of noise and PU's energy, it is important to compare both pdf.

4.4. Obtaining pdf and Performance Metrics

Once the spectrum of interest is sensed, each RFE collects 112 samples with information given in dBm, the mean of the composite signal $\bar{X}(p)$, mean of the noise $\bar{W}(p)$, standard deviation of the composite signal σ_X , and standard deviation of the noise σ_W are calculated and used to plot the pdf.

Repeating the same procedure used for RFE device, and now using the SA, 1005 samples are collected, and then the mean and the standard deviation are calculated and used.

In order to visualize the performance metrics of spectrum sensing, i.e., P_{fa} , P_d , and P_m , we need to consider the pdf curves and T together as shown in Figure 9, and they are formally described next.

False Alarm Probability: P_{fa} refers to the probability that a peak or peaks of the noise signal is detected above T , and it is considered as a real signal of the PU when in reality no PU signal is present. In Figure 9, P_{fa} corresponds to the area bounded by T and $W(p)$ colored with orange.

Detection Probability: P_d is the probability that a real signal of the PU is detected above T , and it is considered as a signal from PU. In Figure 9 it refers to the area bounded by T and $X(p)$ colored with yellow.

Missed-Detection Probability: P_m is the probability that a real signal of the PU is not detected above T , and is considered as noise due to its low amplitude. In Figure 9 it is colored with light-blue.

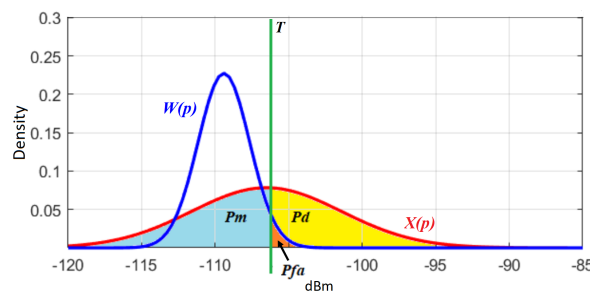


Figure 9. Representation of the P_m , P_{fa} , and P_d , generated by the T and the pdf curves for $W(p)$ and $X(p)$.

4.5. Calculation of Threshold T

In light of the previous discussion, it is evident that T is the most important parameter for accurate sensing, and hence it must be meticulously calculated to permit the balance of P_{fa} and P_d . It is possible to define a minimum limit M_{min} and a maximum limit M_{max} , with M remaining between these values, as follows.

$$M_{min} \leq M \leq M_{max} \quad (8)$$

where M_{min} is obtained by calculating the intersection point of two plotted pdf,

$$M_{min} = W(p) \cap X(p) \quad (9)$$

Note that this is a complex operation considering Equations (6) and (7). The maximum value of M is calculated using

$$M_{max} = \sigma z \quad (10)$$

where σ is the standard deviation of the distribution and z is obtained from the $F(z)$ function, which defines the area under the curve in terms of the standard deviation [32].

To calculate T , the standard deviation and the value of z must be considered. The expression for the noise is given by

$$T = \bar{W}(p) + \sigma_W z_W \quad (11)$$

whereas for the composite signal consisting of signal and noise it is obtained with

$$T = \bar{X}(p) + \sigma_X z_X \quad (12)$$

To obtain T_{min} , it is necessary to solve the equation system (6) and (7) and to eliminate x . The result is expressed in dBm.

To calculate T_{max} , a P_{fa} of 1% is considered according to [13]. Once T is calculated in terms of $\bar{W}(p)$, it is possible to define P_{fa} as follows,

$$P_{fa} = F^{-1}(z_W) \quad (13)$$

With the statistical and probabilistic information of $W(p)$ and $X(p)$, and for a given T , that is common for both pdf curves, the expression for z_X is given by

$$\bar{W}(p) + \sigma_W z_W = \bar{X}(p) + \sigma_X z_X \quad (14)$$

$$z_X = \frac{\bar{W}(p) - \bar{X}(p) + \sigma_W z_W}{\sigma_X} \quad (15)$$

and P_d , related to $X(p)$, is obtained with

$$P_d = F^{-1}(z_X) \quad (16)$$

The information provided by P_{fa} vs P_d , permits to understand the relation between these two probabilities, which defines the optimal value for the proposed adaptive T , as observed in Figure 5b. For both RFE and SA devices, the adaptive T proposed in this research is closer to the $\bar{W}(p)$. In this manner, it avoids missed detections, and observes enough separation, reducing the P_{fa} to a value of 3%. The most important factor is that the proposed adaptive T maintains the same behaviour even if the noise floor or the signal strength experiences any variation.

4.6. Adaptive Threshold

To obtain the adaptive T , two signals (i.e., the noise $W(f)$ and the composite signal $X(f)$) are sensed in parallel in a specific point. From the saved data, the statistical components like mean values and standard deviations are obtained and the pdf are plotted, as shown in Figure 10a. If a T with a P_{fa} of 3% is considered, then $z_W = 1.88$, as shown Figure 10b.

The selected T is common for both normal pdf, i.e., signal and noise. By using Equations (11), (12), (14), and (15), we obtain the value for z_X , whereas P_d is calculated using Equation (16). The relation between P_{fa} and P_d is observed in Figure 10c, which is called the Receiver Operating Characteristics (ROC) curve [33]. Note that P_{fa} for this T is located in the lower part of the axis, so the area of interest for this study is reduced to the light-blue coloured area in the plot. By zooming the area of interest, the maximum values for P_{fa} , re-named as P_{famax} , and the maximum values for P_d , re-named as P_{dmax} , are observed in Figure 10d. Let us consider that P_{dmax} becomes the new highest percentage of signals that may be detected, so the value switches from 56.36% to 99.99% in the Y-axis of the ROC plot.

When we apply Equations (15) and (16), the proposed adaptive T gives 98.57% of detection probability whereas with $M = 5$ dB [25] it is 86.94%. Finally, for 7 dB [26] and 10 dB [34], the detection probability stands at 79.54% or less.

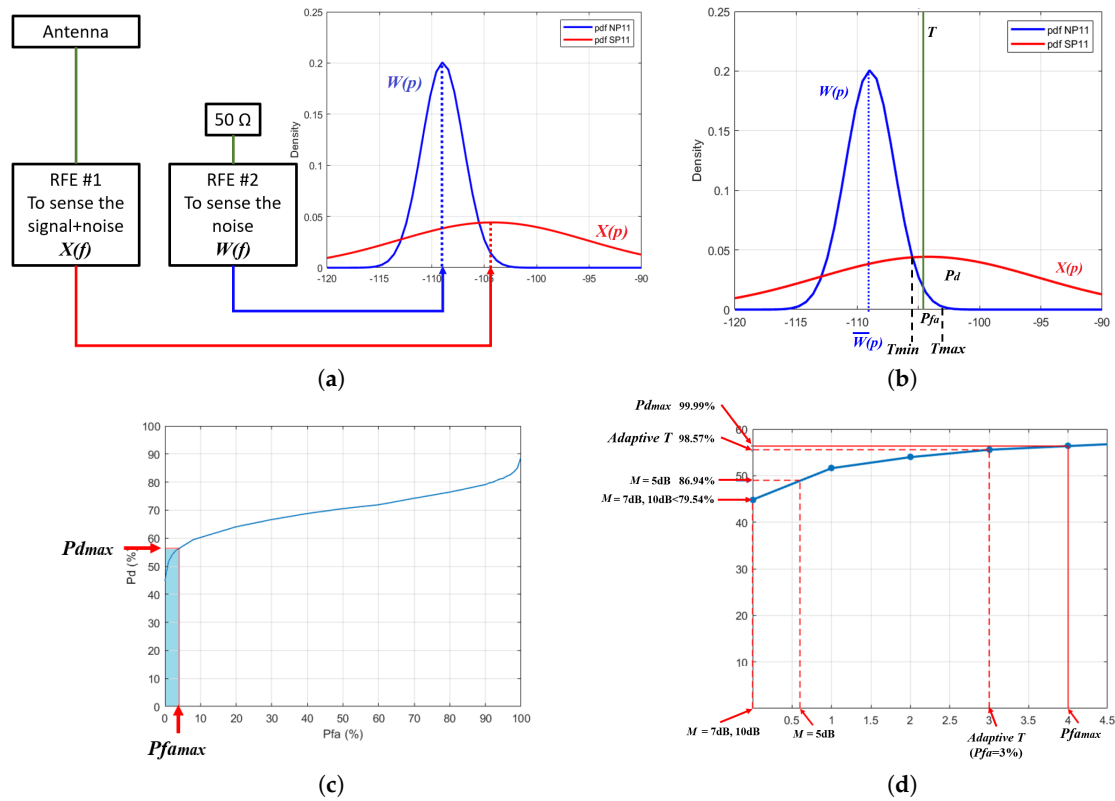


Figure 10. Composite signal and noise sensed in point P11: (a) pdf of the sensed signals; (b) visual representation of a T that observes a $P_{fa} = 3\%$; (c) Detailed Receiver Operating Characteristics (ROC) curve; (d) Re-calculated P_d .

5. Experimental Results and Discussion

In this section, results obtained with the M-SSS scanning the UHF-TV spectrum are presented and discussed. It also explains the different parametric considerations that are needed to accurately distinguish between occupied and idle channels.

5.1. Data Characteristics

As previously mentioned, the value of P_{fa} was selected as 3% for processing the collected data. The obtained results are shown and discussed next.

The M-SSS is mounted on a vehicle to collect the samples. The maximum speed limit (v) in the city at the expressway is 120 Km/h, considering that the RFE takes a sample every 0.340 s (t_s), the maximum distance (d) between two successive samples taken, is given by

$$d = v * t_s \quad (17)$$

and according to this, d is 11.33 m. When the vehicle is travelling faster, this value can decrease according to the speed variations. This maximum distance of the taken samples is small enough to plot the spectrum with an accurate level that represents how the spectrum is being used in the sampled area.

For a particular reading, Figure 11 illustrates: (a) The plot of the spectrum vs power; (b) The pdf of the composed signal combined with the pdf of the noise; And (c) the ROC curve of the P_{fa} vs P_d . This information is used to identify the presence of PU in a sensed band as well as the level of the noise, and it also permits calculation of the adaptive T for each case. This adaptive T is also shown on Figure 11a. In the horizontal axis, channels from 19 to 51 are represented, and vertical the axis corresponds to the absolute power of the signal measured in dBm.

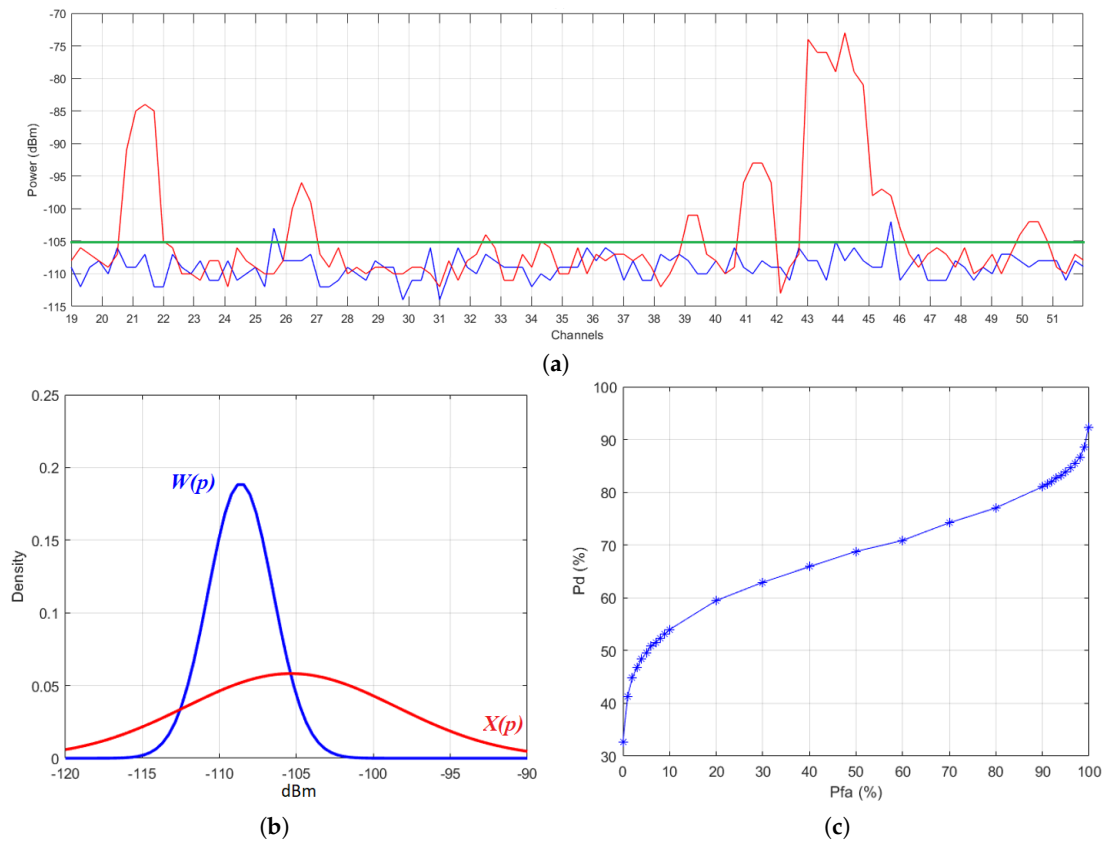


Figure 11. For a specific point sensed: (a) Spectrum diagram; (b) pdf noise and composite signal; and (c) ROC curve with the P_{fa} vs P_d .

Using the same concept of the previously explained figure, Figures 12–14 show the spectrum diagram, pdf of noise and composite signal, and ROC curve, respectively for ten different locations. In Figure 12a, for channel 21 and channels 39–45, we observe that the signal energy is above T . We also observe that some noise peaks are also above T . This reading was taken in a location which is on the eastern end of the city. The subsequent readings were taken in a trajectory that approaches to the central part of the city. In Figure 12b, it is observed that signal energy is detected in channels 31 and 32 in addition to the channels mentioned in Figure 12a. From Figure 12c, it appears that there are energy peaks in channel 50 along with channels 31 and 32, but energy of channel 21 decreases to a level below T . In Figure 12d, the energy of the detected channels maintains its values in relation to the previous figure. In Figure 12e there are well-defined peaks of energy in channels 20–21, 26, 31–32, 38 to 46, and 50. In Figure 12f, the profile is maintained, the general levels of energy decreases, but the same channels are detected. For Panels (g), (h), (i), and (j), the detected energy does not present any significant variation and it is the usual energy profile of the channels detected in the central area of the city. The channels detected are 20–21, 25–26, 31–32, 38 to 46, and 50.

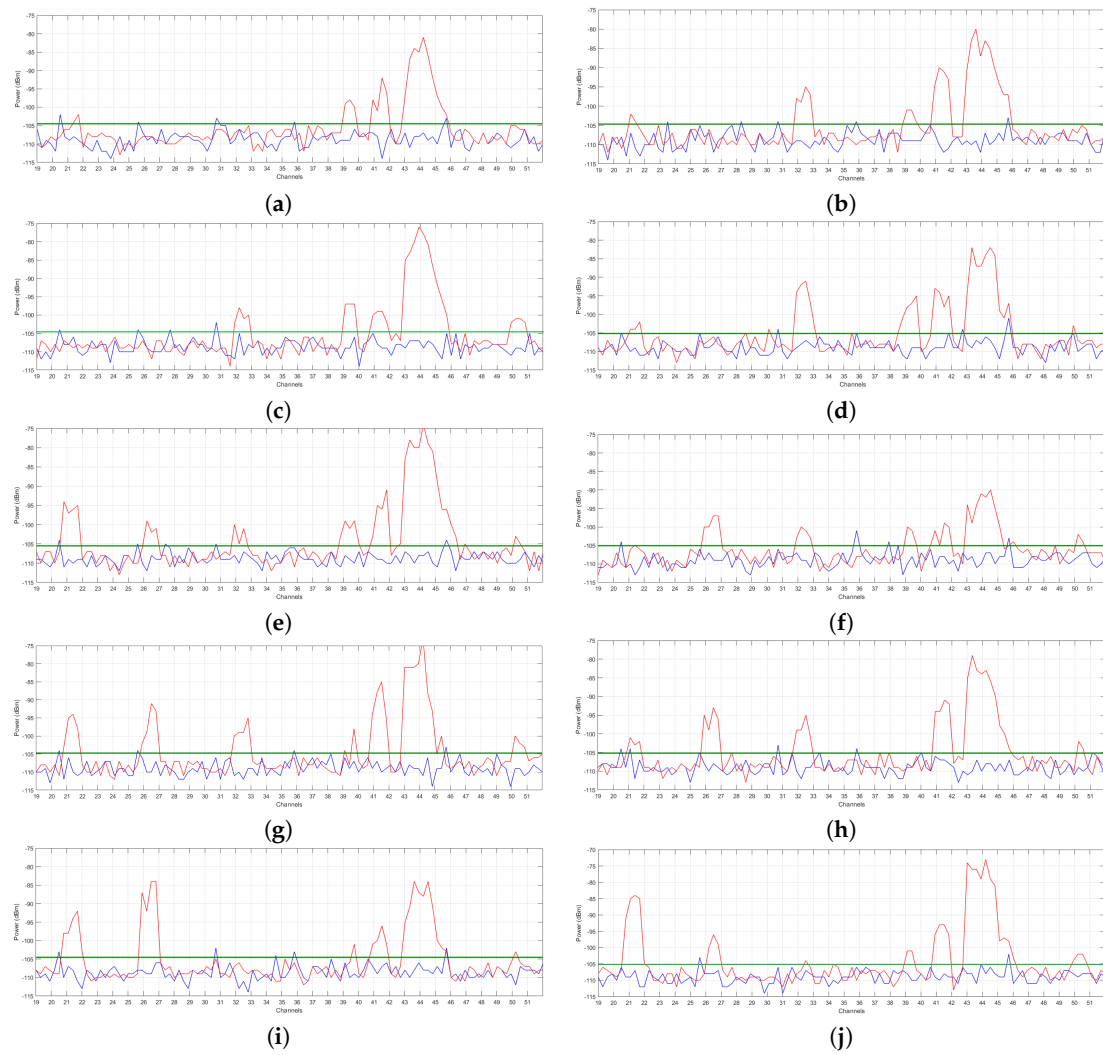


Figure 12. $W(f)$ and $X(f)$ represented in the frequency domain. Panels (a–j) spectrum vs power sensed in Points 1–10, there are variations on the energy detected due to the different location in which the samples were taken.

For the next block of plots in Figure 13, the pdf of the noise $W(f)$ and the composite signal $X(f)$ are shown. Their relative amplitudes and positions vary depending on the presence of energy and noise detected. These small variations mark the difference that determined to set adaptive T for each case.

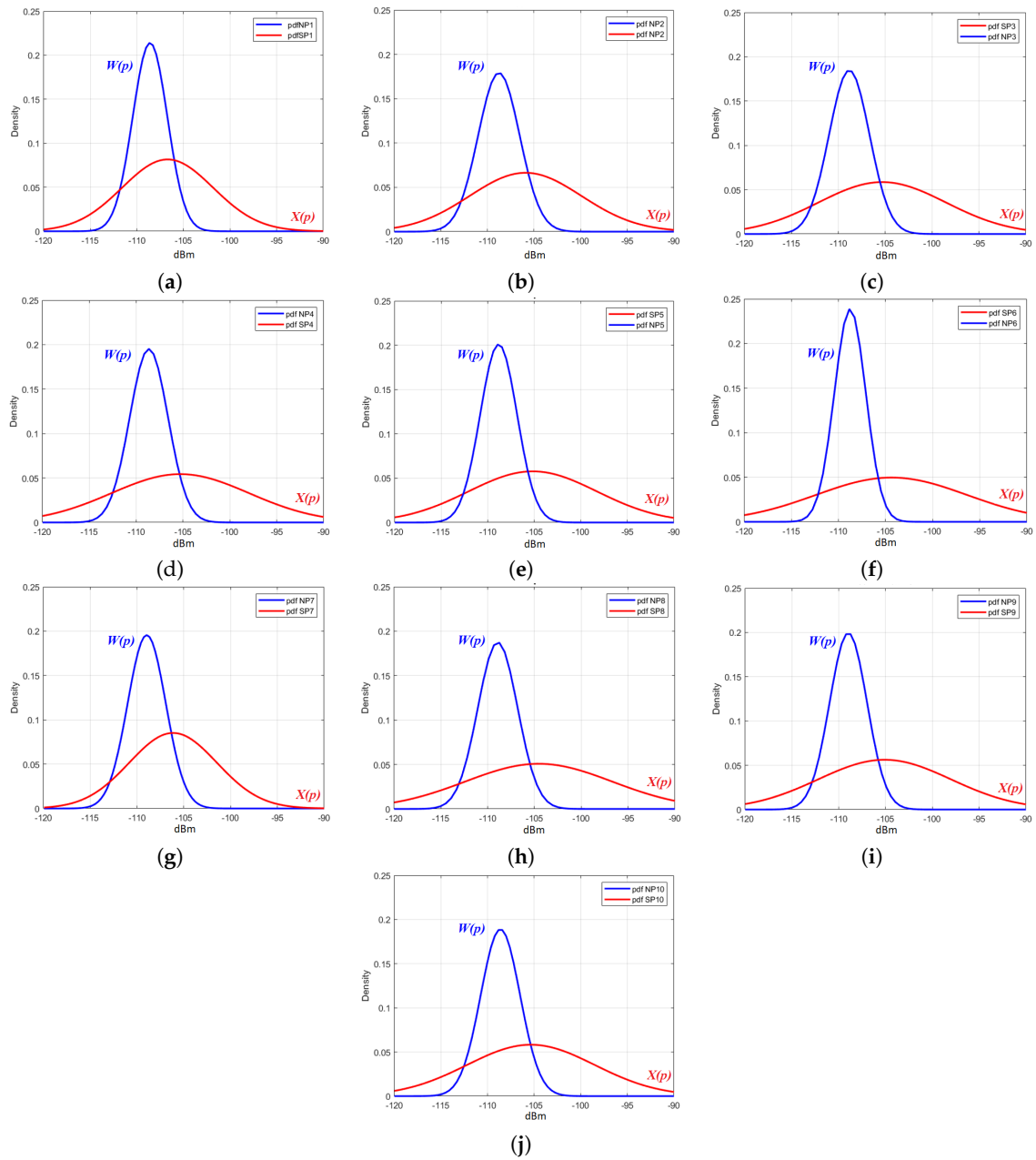


Figure 13. Each Panel contains a plot of the pdf of the signals sensed, from (a–j) pdf of the $W(f)$ and $X(f)$ taken in Points 1–10.

In Figure 14, the ROC curves from each of the ten locations are plotted. These curves represent the relation between P_{fa} and P_d in each case. The different values respond to the variations previously registered in the sensed locations. These curves have enough information to reveal the behaviour of the spectrum.

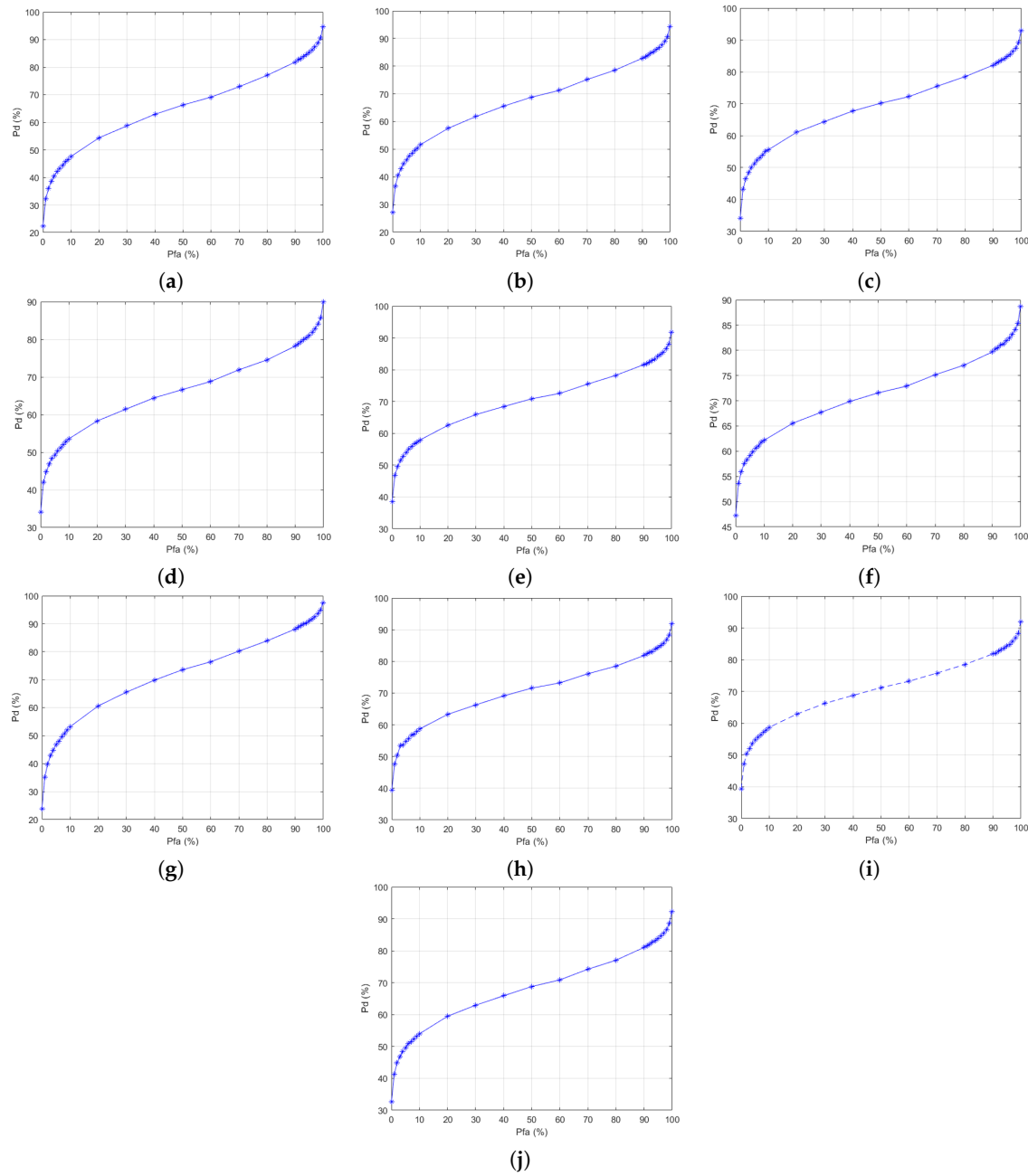


Figure 14. ROC that represents the relation of P_{fa} vs. P_d . Panels (a–j) ROC curves of the signal sensed in Points 1 to 10.

It is important to note that each reading provides valuable information to determine the state of the spectrum in that specific location at an instant of time t_i . To obtain a global view of the proposed method and its applicability, it is necessary to compare all the obtained curves together to find a usable relationship, if any. Figure 15a plots the ROC curves (P_{fa} vs P_d) of the ten analyzed locations. It is quite clear that each location has its own characteristics which differ from others. Figure 15b depicts the same ROC curves shown in Figure 15a but focusing on a P_{fa} a range of 0% to 4%. Additionally, the dotted vertical lines represent the adaptive T in red, the T obtained with a $M = 5$ dBm in blue, $M = 7$ dBm in green, and $M = 10$ dBm in brown, respectively. The Y-coordinate value of the intersection of a particular T and the ROC curve of a location represents P_d . For example in P3, for a P_{fa} of 3%, it corresponds to a 48.4% of P_d according to the vertical-axis scale of the ROC plot, and it means a 96.8% of the P_{dmax} .

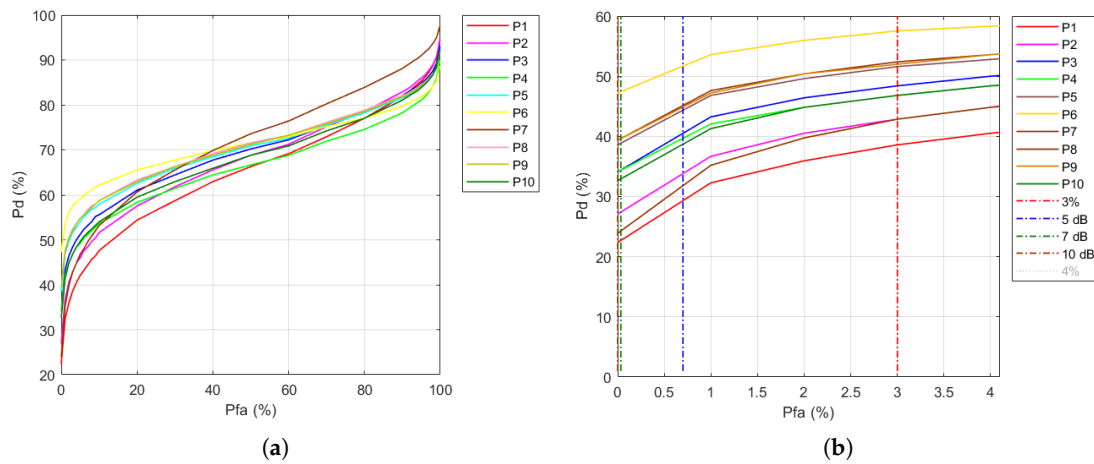


Figure 15. ROC curves obtained from P1–P10, in (a) are present all the curves, and in (b) are shown the same plot but zooming in to observe the curves with a P_{fa} closer to the one defined by the adaptive T of 3%.

To visualize the accuracy of the model that proposes an adaptive T , the curve of the P_{fa} vs P_d is obtained by calculating the average of 36,176 readings or 4,051,712 samples. By using Equations (5), (9), (15), and (16), the P_{famax} is obtained and it corresponds to 4%. Figure 16 illustrates the average curve, the P_{famax} , the adaptive T , and the values for T using a margin M of 5, 7, and 10 dB. Considering that P_{famax} defines the P_{dmax} which becomes 99.99% of the signals that are possible to be detected, then the values of the Y-axis were re-calculated according to the new P_{dmax} scale. In gray color it can be observed the recommended operation area, defined by the P_{famax} , P_{famin} , P_{dmax} , and P_{dmin} , and on the left side of the plot, are the new re-calculated values for P_d .

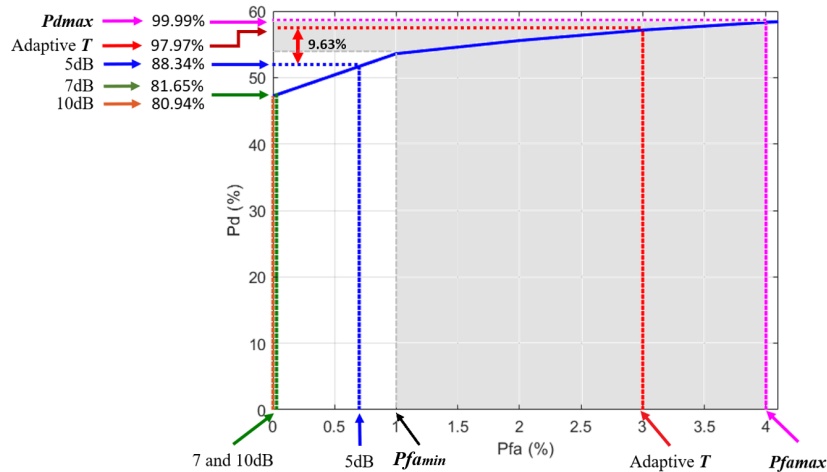


Figure 16. Dotted lines are the P_{famax} , P_{fa} calculated with the adaptive T , and T obtained by using a M of 5, 7, and 10 dB respectively. It is observed that the adaptive T proposed increases at least 9.63% of P_d than the values used by other authors.

5.2. Discussing the Results

In this project, 33 UHF-TV channels (Channel 19 to channel 51), each having a bandwidth of 6 MHz, were sensed. Channel 37 is assigned to radio astronomy and it is not used for TV broadcast, so that results were obtained for the remaining 32 TV channels. According to the information collected and applying the proposed model, six channels were found to have enough energy above T and the PU presence was confirmed. In Figure 17, the geographical points are plotted in which their occupation is represented.

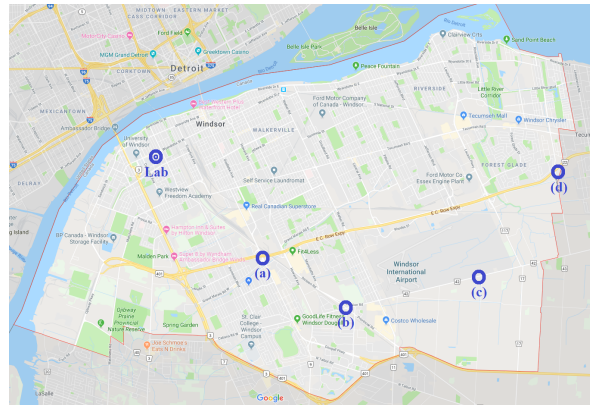


Figure 17. Location of the represented points.

5.3. Spectrum Sensed Results

In this sub-section, the obtained results are described. Figure 17 illustrates five locations, i.e., *Lab*, (a), (b), (c), and (d), where data were sensed and represented. In *Lab*, we found the existence of PU in 23 channels, so it shows 72% of TV spectrum used and 28% idle spectrum. The later may be considered as potentially TVWS allowing DSA as SU. In Figure 18a, the results are plotted for data taken in location (a), where we observe seventeen channels for which signal was detected (in cyan), so that this is 53% of TV spectrum used, and 47% idle spectrum. Figure 18b corresponds to location (b) to the South of the city, where there are 16 channels for which signal was detected (in cyan), representing 50% of used spectrum, and 50% of TVWS. In Figure 18c, which is the Middle-east part of the city, there are 15 channels for which signal was detected, which represents 50% of the used spectrum, and 50% of TVWS. Finally, in Figure 18d, which shows the East limit of the city, there are 13 channels for which signal was detected by the DAI (in cyan) so that this represents 40% of used spectrum and 60% of TVWS.

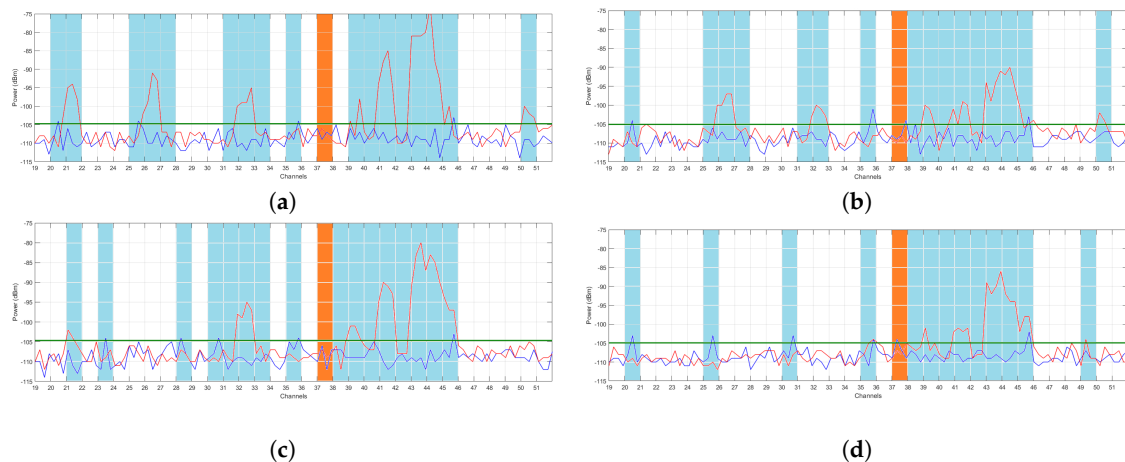


Figure 18. Spectrum detected and analyzed with the proposed model: (a) Central south part of the city, (b) South-east, (c) Middle East, and (d) Eastern limit of the city of Windsor. Note that as far of the center the sample is taken, less PUs are detected.

5.4. Variability of the Sensed Signals

The reason to take simultaneous samples of the noise $W(p)$ and the composite signal $X(p)$ at each time instant t_i , responds to the variations experienced in the UHF-TV spectrum by the above-mentioned signals. In Figure 19 we can observe the pdf of the average values for $W(p)$ and $X(p)$. To obtain this pdf, from trajectory T2, 1,166,928 samples were collected. The mean values of the signals were obtained, and a CI corresponding to 95% was calculated and plotted. Figure 19 also shows that the noise mean

$\bar{W}(p)$ has a value of -108.9725 and can have a variation of 1.05 dB. The mean of the composite signal $\bar{X}(p)$ has a value of -103.9889 with a CI of 6.72 dB.

Around $\bar{X}(p)$, represented with a red dashed line, the mean of the composite signal values, could vary in 6.72 dB. Now, it means that sometimes the respective pdf of the noise and the composite signal may be closer or separated from each other. This variation is confirmed by the plots represented in Figure 13. In order to avoid any error produced by the variation mentioned above, it is recommended to obtain separate readings for signal and noise. This is more applicable when the M-SSS is used and the samples are taken in different geographical locations every t_i .

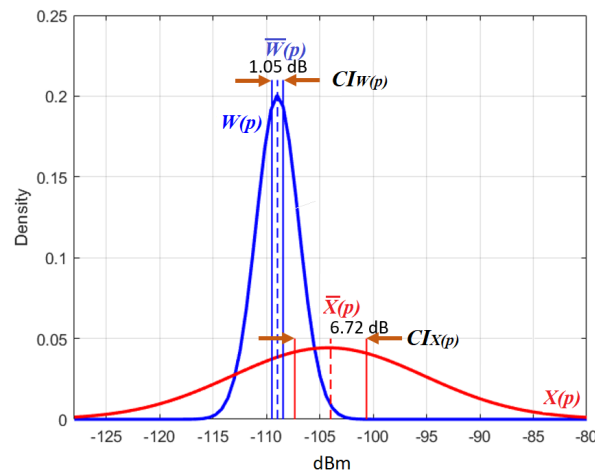


Figure 19. Confidence Interval (CI) of average values for $W(p)$ and $X(p)$, the variations are represented in dB.

5.5. Processing Time

According to Figure 3, the proposed model has six blocks in which the information of the UHF-TV spectrum is collected and processed. The action performed in each block, a brief explanation, and its respective average time is summarized in Table 4.

Table 4. Average time obtained in each block of the proposed model.

Block	Action Performed	Observations	Time
①	Spectrum sensing	Antenna/RFE collect samples $W(f)$, $X(f)$	0.00 s
②	Samples processing	Two RFE save samples in DB	0.34 s
③	Statistical calculations	Matlab \rightarrow calculates $\bar{W}(f)$, σ_W , $\bar{X}(f)$, and σ_X	0.31 s
④	Probability calculations	With a selected P_{fa} , Matlab \rightarrow calculates M and T	0.24 s
⑤	ED performing	Matlab \rightarrow $\bar{X}(f)$ is compared with T	0.27 s
⑥	Results presentation	Channel's energy lower than T are marked as TVWS	0.29 s
Total			1.45 s

For blocks ① and ②, the time of the collected samples saved in the DB was obtained using the RF Explorer for Windows open software. For blocks ③ to ⑥, the time was calculated in the Matlab script by using the start stopwatch timer command and running 500 times the mentioned script. To reduce the time in block ④, we do not calculate the intersection point of two pdf curves W and X , in this case, we use the value of P_{fa} corresponding to 3%, and performing the operation explained in Equation (11), obtaining the value of T .

The total average time to find the TVWS in one reading is 1.45 s. To reduce it according to the detection time suggested in the 802.22 standards [10], it is possible to use big data processing techniques or use hardware with improved processing frequency, to achieve real-time detection.

6. Conclusions

A probabilistic model for identifying TVWS has been proposed. The model was based on the probabilistic analysis performed on collected spectrum information in the city of Windsor, Canada. To collect the spectrum information over a wide geographical area, a vehicle-mounted M-SSS was designed and implemented. It uses light weight components, consumes low power, and is easy to handle.

A noteworthy feature of the M-SSS is that it uses two RFE devices connected in parallel for sensing the composite signal $X(f)$ and noise signal $W(f)$ simultaneously. This individual sensing enables our model to yield better accuracy. Based on this simultaneously sensed data, the model uses two statistical parameters, i.e., the false alarm probability and the detection probability to calculate an adaptive threshold.

The false alarm probability and the detection probability values are calculated based on the consideration that both the noise signal and the composite signal follow Normal distribution. In reality, the noise signal truly follows a Normal distribution as verified by the Kolmogorov–Smirnov test performed in our work, but the composite signal actually is a multi modal signal. In order to reduce computational complexity related to probabilistic analysis, the composite signal has also been assumed to follow the Normal distribution. We consider this assumption is acceptable, and it does not hamper the detection accuracy of our model. This is because the fundamental calculations involved in finding the false alarm probability is based only on the noise signal, which as mentioned before, indeed follows a Normal distribution. The optimal false alarm probability is used as an input in the receiver operating characteristic curve function, and the optimal detection probability is obtained.

In terms of performance, the proposed model demonstrates about 9.6% higher detection probability (P_d) compared to other methods found in literature. From our collected data, we observed that in the central area of the city, about 28% of the sensed spectrum are TVWS and as we move to the outer edges of the city, up to 60% of the TV channels sensed were found to be TVWS.

This observation clearly suggests that there lies a significant number of unused TV channels which can be used for different opportunistic services through the implementation of cognitive radio-enabled dynamic spectrum access. Finally, it can be concluded that the proposed mobile spectrum sensing station along with the proposed probabilistic model for sensing the UHF-TV spectrum may be used in any other location.

Author Contributions: D.C.-D.-W. collected and organized the data presented in this paper and analyzed the information. D.C.-D.-W., S.A. and J.L.R.-A. wrote and reviewed the manuscript, analyzing the most relevant data. F.A. and K.T. reviewed and discussed the manuscript.

Acknowledgments: This work was supported by the Secretaría de Educación Superior, Ciencia, Tecnología e Innovación de Ecuador and the *University of Windsor*. Authors thank to the WiCIP Lab for providing all the equipment necessary to collect the information which is analyzed and discussed in this manuscript.

Conflicts of Interest: The authors declare no conflict of interest.

References

1. Liang, Y.C.; Chen, K.C.; Li, G.Y.; Mahonen, P. Cognitive radio networking and communications: An overview. *IEEE Trans. Veh. Technol.* **2011**, *60*, 3386–3407. [\[CrossRef\]](#)
2. Datla, D.; Wyglinski, A.M.; Minden, G.J. A spectrum surveying framework for dynamic spectrum access networks. *IEEE Trans. Veh. Technol.* **2009**, *58*, 4158–4168. [\[CrossRef\]](#)
3. Liu, Y.; Ding, Z.; Elkashlan, M.; Yuan, J. Nonorthogonal multiple access in large-scale underlay cognitive radio networks. *IEEE Trans. Veh. Technol.* **2016**, *65*, 10152–10157. [\[CrossRef\]](#)
4. Brown, T.X.; Pietrosemoli, E.; Zennaro, M.; Bagula, A.; Mauwa, H.; Nleya, S.M. A survey of TV white space measurements. In *International Conference on e-Infrastructure and e-Services for Developing Countries*; Springer: Berlin/Heidelberg, Germany, 2014; pp. 164–172.
5. Shellhammer, S.J. Spectrum Sensing in IEEE 802.22. In *Proceedings of the IAPR Workshop on Cognitive Information Processing*, Santorini, Greece, 9–10 June 2008; pp. 9–10.

6. Mitola, J.; Maguire, G.Q. Cognitive radio: Making software radios more personal. *IEEE Pers. Commun.* **1999**, *6*, 13–18. [CrossRef]
7. Haykin, S. Cognitive radio: Brain-empowered wireless communications. *IEEE J. Sel. Areas Commun.* **2005**, *23*, 201–220. [CrossRef]
8. Cordeiro, C.; Challapali, K.; Birru, D.; Shankar, S. IEEE 802.22: An introduction to the first wireless standard based on cognitive radios. *J. Commun.* **2006**, *1*, 38–47.
9. Rusch, L.A. Indoor wireless communications: Capacity and coexistence on the unlicensed bands. *Int. Technol. J.* **2001**, *3*, 2001.
10. IEEE. IEEE 802.22 Working Group on Wireless Regional Area Networks. Available online: <http://www.ieee802.org/22/> (accessed on 31 March 2019).
11. Zeng, Y.; Liang, Y.C. Eigenvalue-based spectrum sensing algorithms for cognitive radio. *IEEE Trans. Commun.* **2009**, *57*, 1784–1793. [CrossRef]
12. Pietrosemoli, E.; Zennaro, M. TV White Spaces—A Pragmatic Approach. In Proceedings of the Sixth International Conference on Information and Communication Technologies and Development, Cape Town, South Africa, 7–10 December 2013.
13. Chen, Y.; Oh, H.S. A survey of measurement-based spectrum occupancy modeling for cognitive radios. *IEEE Commun. Surv. Tutor.* **2016**, *18*, 848–859. [CrossRef]
14. Manesh, M.R.; Subramaniam, S.; Reyes, H.; Kaabouch, N. Real-time spectrum occupancy monitoring using a probabilistic model. *Comput. Netw.* **2017**, *124*, 87–96. [CrossRef]
15. Akyildiz, I.F.; Lee, W.Y.; Vuran, M.C.; Mohanty, S. NeXt generation/dynamic spectrum access/cognitive radio wireless networks: A survey. *Comput. Netw.* **2006**, *50*, 2127–2159. [CrossRef]
16. Federal Communications Commission (FCC). Docket No 03-222 Notice of Proposed Rule Making and Order. Available online: <https://web.cs.ucdavis.edu/~liu/289I/Material/FCC-03-322A1.pdf> (accessed on 26 September 2019).
17. Jing, X.; Raychaudhuri, D. Spectrum co-existence of IEEE 802.11 b and 802.16 a networks using the CSCC etiquette protocol. In Proceedings of the First IEEE International Symposium on New Frontiers in Spectrum Access Networks, Baltimore MD, USA, 8–11 November 2005; pp. 243–250.
18. Akhtar, F.; Rehmani, M.H.; Reisslein, M. White space: Definitional perspectives and their role in exploiting spectrum opportunities. *Telecommun. Policy* **2016**, *40*, 319–331. [CrossRef]
19. International Telecommunications Union (ITU). Frequency Bands allocated to Terrestrial Broadcasting Services. Available online: <https://www.itu.int/en/ITU-R/terrestrial/broadcast/Pages/Bands.aspx> (accessed on 26 September 2019).
20. Corral-De-Witt, D.; Younan, A.; Fatima, A.; Matamoros, J.; Awin, F.A.; Tepe, K.; Abdel-Raheem, E. Sensing tv spectrum using software defined radio hardware. In Proceedings of the 2017 IEEE 30th Canadian Conference on Electrical and Computer Engineering (CCECE), Windsor, ON, Canada, 30 April–3 May 2017; pp. 1–4.
21. Awin, F.; Younan, A.; Corral-De-Witt, D.; Tepe, K.; Abdel-Raheem, E. Real-Time Multi-Channel TVWS Sensing Prototype Using Software Defined Radio. In Proceedings of the 2018 IEEE International Symposium on Signal Processing and Information Technology (ISSPIT), Louisville, KY, USA, 6–8 December 2018; pp. 212–217.
22. RF Explorer. RF Explorer Spectrum Analyzer. Available online: <http://j3.rf-explorer.com/40-rfe/article/48-introducing-rf-explorer> (accessed on 29 March 2019).
23. Tektronix. MDO 4000 Series Manual. Available online: <https://www.tek.com/oscilloscopes/mdo4000-manual/mdo4000-series-0> (accessed on 29 March 2019).
24. Lekontsev, D.; Maršálek, R. Comparison of 802.11 af and 802.22 standards—physical layer and cognitive functionality. *Elektro Revue* **2012**, *3*, 12–18.
25. Harrold, T.; Cepeda, R.; Beach, M. Long-term measurements of spectrum occupancy characteristics. In Proceedings of the 2011 IEEE International Symposium on Dynamic Spectrum Access Networks (DySPAN), Aachen, Germany, 3–6 May 2011; pp. 83–89.
26. Valenta, V.; Maršálek, R.; Baudoin, G.; Villegas, M.; Suarez, M.; Robert, F. Survey on spectrum utilization in Europe: Measurements, analyses and observations. In Proceedings of the 2010 Fifth International Conference on Cognitive Radio Oriented Wireless Networks and Communications, Cannes, France, 16–18 June 2010; pp. 1–5.

27. Qaraqe, K.A.; Celebi, H.; Gorcin, A.; El-Saigh, A.; Arslan, H.; Alouini, M.S. Empirical results for wideband multidimensional spectrum usage. In Proceedings of the 2009 IEEE 20th International Symposium on Personal, Indoor and Mobile Radio Communications, Tokyo, Japan, 13–16 September 2009; pp. 1262–1266.
28. Awin, F.; Abdel-Raheem, E.; Tepe, K. Blind spectrum sensing approaches for interweaved cognitive radio system: A tutorial and short course. *IEEE Commun. Surv. Tutor.* **2019**, *21*, 238–259. [CrossRef]
29. Awin, F.A.; Alginahi, Y.M.; Abdel-Raheem, E.; Tepe, K. Technical Issues on Cognitive Radio-Based Internet of Things Systems: A Survey. *IEEE Access* **2019**, *7*, 97887–97908. [CrossRef]
30. Chambers, J.M. *Graphical Methods for Data Analysis: 0*; Chapman and Hall/CRC: Boca Raton, FL, USA, 2017.
31. Massey, F.J., Jr. The Kolmogorov–Smirnov test for goodness of fit. *J. Am. Stat. Assoc.* **1951**, *46*, 68–78. [CrossRef]
32. Z Table. Z Score Table. Available online: <http://www.z-table.com/> (accessed on 18 April 2019).
33. Brown, C.D.; Davis, H.T. Receiver operating characteristics curves and related decision measures: A tutorial. *Chemom. Intell. Lab. Syst.* **2006**, *80*, 24–38. [CrossRef]
34. International Telecommunications Union ITU. Handbook Spectrum Monitoring, Chapter 3. Available online: <https://extranet.itu.int/brdocsearch/R-HDB/R-HDB-23/R-HDB-23-2002/R-HDB-23-2002-OAS-PDF-E.pdf> (accessed on 29 March 2019).



© 2019 by the authors. Licensee MDPI, Basel, Switzerland. This article is an open access article distributed under the terms and conditions of the Creative Commons Attribution (CC BY) license (<http://creativecommons.org/licenses/by/4.0/>).